The N-terminal TOG domain of *Arabidopsis* MOR1 modulates affinity for microtubule polymers

Bettina Lechner[1],*, Madeleine C. Rashbrooke[2],*, David A. Collings[2,3], Ryan C. Eng[1], Eiko Kawamura[1], Angela T. Whittington[2] and Geoffrey O. Wasteneys[1,2,‡]

[1]Department of Botany, University of British Columbia, Vancouver, BC V6T 1Z4, Canada
[2]Research School of Biology, Australian National University, Canberra, ACT 0200, Australia
[3]School of Biological Sciences, University of Canterbury, Christchurch 8140, New Zealand

*These authors contributed equally to this work
‡Author for correspondence (geoffrey.wasteneys@ubc.ca)

Summary

Microtubule-associated proteins of the highly conserved XMAP215/Dis1 family promote both microtubule growth and shrinkage, and move with the dynamic microtubule ends. The plant homologue, MOR1, is predicted to form a long linear molecule with five N-terminal TOG domains. Within the first (TOG1) domain, the *mor1-1* leucine to phenylalanine (L174F) substitution causes temperature-dependent disorganization of microtubule arrays and reduces microtubule growth and shrinkage rates. By expressing the two N-terminal TOG domains (TOG12) of MOR1, both *in planta* for analysis in living cells and in bacteria for *in vitro* microtubule-binding and polymerization assays, we determined that the N-terminal domain of MOR1 is crucial for microtubule polymer binding. Tagging TOG12 at the N-terminus interfered with its ability to bind microtubules when stably expressed in *Arabidopsis* or when transiently overexpressed in leek epidermal cells, and impeded polymerase activity *in vitro*. In contrast, TOG12 tagged at the C-terminus interacted with microtubules *in vivo*, rescued the temperature-sensitive *mor1-1* phenotype, and promoted microtubule polymerization *in vitro*. TOG12 constructs containing the L174F *mor1-1* point mutation caused microtubule disruption when transiently overexpressed in leek epidermis and increased the affinity of TOG12 for microtubules *in vitro*. This suggests that the *mor1-1* mutant protein makes microtubules less dynamic by binding the microtubule lattice too strongly to support rapid plus-end tracking. We conclude from our results that a balanced microtubule affinity in the N-terminal TOG domain is crucial for the polymerase activity of MOR1.

Key words: XMAP215, MOR1, TOG domain, HEAT repeat, *Mor1-1*, Microtubule-associated protein, Microtubule affinity

Introduction

The essential role microtubules play in plant development, including determination of cell division planes and the direction of cell expansion, is defined by the ability of microtubules to self-organise into distinct arrays as cells progress through the cell cycle. This self-organisation relies on the ability of microtubules to assemble and disassemble rapidly (Wasteneys and Ambrose, 2009), which is governed, to a large extent, by one essential protein, MOR1.

MOR1 is a member of the Dis1/TOG protein family, which includes orthologues in all eukaryotes (Gard et al., 2004). Comparative sequence analysis shows that the most highly conserved features of XMAP215/Dis1 proteins are the N-terminal TOG domains, named after the homologous human protein tumour overexpressed gene (Charrasse et al., 1998), each of which are about 250 amino acids in length. Most orthologues, including MOR1, have five TOG domains as well as a conserved C-terminal domain but in nematodes and yeasts, the number of TOG domains has been reduced to three and two, respectively, and the C-terminal regions are divergent. Both GFP tagging (Popov et al., 2001) and antibody labelling (Tournebize et al., 2000) localise *Xenopus laevis* MAP215 (XMAP215) to interphase microtubules and spindle fibres. Depending on the cell type and stage of cell cycle, XMAP215/Dis1 proteins

can promote plus-end microtubule polymerization, antagonize kinesin-dependent microtubule depolymerization and increase microtubule catastrophes. Brouhard et al. showed that XMAP215 works as a processive microtubule polymerase *in vitro*, for which both simultaneous binding to microtubules and tubulin, and being able to move with the growing end of microtubules, are important (Brouhard et al., 2008). Although some amino acids that are important for microtubule and tubulin binding have been identified, the mechanism of plus-end tracking remains unknown.

Positively charged regions adjacent to TOG domains have been identified as microtubule-binding domains (MBD) (Gard et al., 2004; Currie et al., 2011; Widlund et al., 2011) and are likely to interact with negatively charged residues at the C-terminus of tubulin, the so-called E-hook. It remains unclear whether these domains are conserved in quantity and quality among species. The TOG domains themselves are also important for binding tubulin. According to X-ray crystallography, TOG domains form flattened, paddle-like structures, each consisting of six HEAT repeats stacked side by side (Al-Bassam et al., 2007; Slep and Vale, 2007). Each HEAT repeat is an α-helix–turn–α-helix motif, with the turns building a narrow edge of the paddle. Conserved amino acid residues along this narrow face are required for interaction with tubulin dimers (Al-Bassam et al., 2007; Slep and Vale, 2007), although this does not seem to be

true for all TOG domains. While mutations in these conserved amino acids in TOG 1 and 2 of XMAP215 reduced the tubulin affinity of the whole protein, equivalent mutations in TOG 3, 4 and 5 did not (Widlund et al., 2011). Variations in the conserved intra-HEAT repeat turns may, therefore, modulate affinity for free tubulin (reviewed by Al-Bassam and Chang, 2011).

The microtubule- and tubulin-binding domains of MOR1 have not been thoroughly investigated. Partial purification of the MOR1 homologue TMB200/MAP200 from cultured *Nicotiana tabacum* cells enabled preliminary *in vitro* studies to be conducted (Hamada et al., 2004; Hamada et al., 2009). A polypeptide expressed from an *Arabidopsis* cDNA encoding the C-terminal 800 amino acids of MOR1 co-pelleted with microtubules, confirming that the C-terminus can confer binding to microtubule polymers (Twell et al., 2002). So far, no regions other than the C-terminus of MOR1 have been tested for interaction with microtubules.

The function of MOR1 in plant cells has been largely inferred from the phenotypes of three mutant alleles with single amino acid substitutions, identified by forward genetic screens in *Arabidopsis thaliana* (Whittington et al., 2001; Konishi and Sugiyama, 2003). All three mutations substitute conserved amino acids in the first N-terminal TOG domain of the 217 kDa MOR1 protein and give rise to temperature-sensitive disorganization of microtubule arrays (Whittington et al., 2001; Konishi and Sugiyama, 2003; Eleftheriou et al., 2005; Kawamura et al., 2006). The *mor1-1* (L174F) allele located in the α-helix of the fifth HEAT repeat of TOG1 causes temperature-dependent reduction in microtubule growth and shrinkage rates (Kawamura and Wasteneys, 2008). Immunofluorescence demonstrates that the mutant mor1-1 protein remains bound to microtubules at the restrictive temperature, suggesting that the loss of function is not mediated through weakened association with the microtubule polymer (Kawamura et al., 2006). Point mutations in the fifth HEAT repeat have been found to be important for proper protein function in yeast (Wang and Huffaker, 1997), nematodes (Bellanger et al., 2007) and flies (Brittle and Ohkura, 2005), underlining the probability that members of the XMAP215/Dis1 family work with very similar mechanisms.

Two recent publications suggest that the first two TOG domains can work like the full-length protein, although less efficiently (Currie et al., 2011; Widlund et al., 2011). Currie et al. showed that the first two TOG domains exhibit partial rescue of the MSPS RNAi phenotype *in vivo*, and Widlund et al. reported that TOG12 works as a 'bonsai polymerase' *in vitro* (Currie et al., 2011; Widlund et al., 2011). Thus, to advance the understanding of the conserved mechanisms by which XMAP215/Dis1 proteins control microtubule dynamics, analysis of the two N-terminal TOG domains (TOG12) is likely to be useful.

In this study, we expressed variants of the two N-terminal TOG domains of MOR1 *in planta* for analysis in living cells, and in bacteria for *in vitro* microtubule-binding and polymerization assays with recombinant protein. We show that tagging TOG12 at the N-terminus interferes with its ability to bind microtubule polymers and abolishes *in vitro* polymerase activity. In contrast, when tagged at the C-terminus, TOG12 associated with microtubules *in vivo*, rescued the *mor1-1* temperature-sensitive phenotype, and promoted microtubule polymerization *in vitro*. Intriguingly, the presence of the *mor1-1* point mutation in the TOG12 fragment caused microtubule disruption when transiently overexpressed in leek epidermal cells, and increased the affinity of TOG12 for microtubules during *in vitro* assays. These findings

underline the importance of the N-terminus of the XMAP215/ Dis1 family for microtubule binding as well as tubulin polymerase activity and shed light on how mutations in the 5th HEAT repeat of the N-terminal TOG domain cause loss of function.

Results
Stable expression of YFP–TOG12 constructs in *Arabidopsis* shows variable levels of expression and no microtubule labelling

To investigate the nature of interaction between microtubules and the highly conserved N-terminal TOG1 and TOG2 domains of MOR1 (hereafter referred to as TOG12), we generated gene constructs for fluorescence imaging (Fig. 1). The gene fragment encoding the first 509 amino acids of MOR1 was cloned from cDNA, obtained either from wild-type or *mor1-1* (L174F) plants. We ligated TOG12 and TOG12^{mor1-1} at the 5′ end to the sequence encoding yellow fluorescent protein (YFP) downstream of the cauliflower mosaic virus 35S promoter. After transformation, we analysed multiple, independent kanamycin-resistant *Arabidopsis* T1 plants for each YFP–TOG12 construct. Analysis of T2 lines showed consistent, construct-specific differences in fluorescence levels (Fig. 2A,B) that were inherited in subsequent generations. Interestingly, the fluorescence of YFP–TOG12^{mor1-1} lines was consistently low, whereas YFP–TOG12 and the YFP control showed moderate and high levels of fluorescence, respectively (Fig. 2A, red bars). When analysed by confocal microscopy, YFP was present in both the cytoplasm and nucleus, while the YFP–TOG12 fragments were cytoplasmically localised but excluded from the nucleus. No microtubule labelling was evident (Fig. 2B).

We used quantitative real-time PCR to determine gene expression of both *YFP-TOG12* constructs and the *YFP* control (Fig. 2A, blue bars). Despite the low level of YFP–TOG12^{mor1-1} fluorescence, *YFP* RNA levels (Fig. 2A, yellow bars) were similar in the *YFP-TOG12^{mor1-1}* and *YFP-TOG12* wild-type transformants. We conclude that *YFP-TOG12^{mor1-1}* was
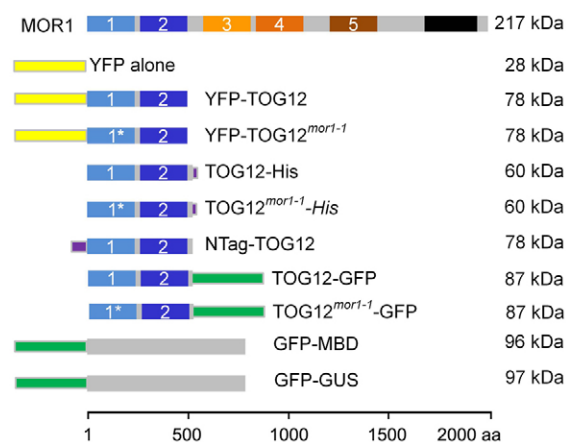

Fig. 1. Schematic representations of fusion constructs. The first two N-terminal TOG domains (blue) of MOR1 were fused to four different tags: YFP, His, an 18 kDa N-terminal affinity tag (N-tag) and GFP. The mor1-1 L174F point mutation is indicated by an asterisk in the first TOG domain. Full-length MOR1 is shown for comparison. As controls, cytoplasmic YFP, GFP–GUS as a large cytosolic protein and GFP–MBD as a microtubule-labelling construct were used. YFP fusion protein is shown in yellow and GFP in green; tags for affinity purification are purple.
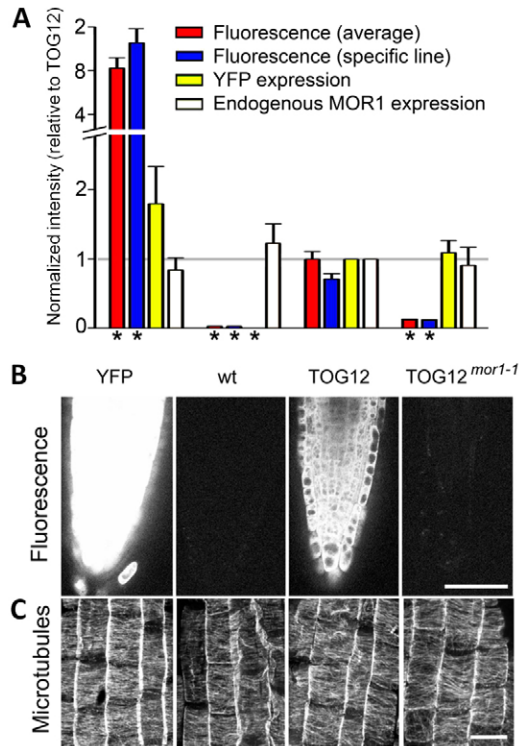
Fig. 2. Stable transformation of *Arabidopsis* with YFP-TOG12 constructs. (**A**) Multiple (*n*=3–8) stable transformants were recovered for each *YFP-TOG12* construct. Using wide-field microscopy, fluorescence in the root tip was averaged in 7-day-old plants (data normalised against YFP–TOG12; values are means ± s.e.m.; red bars). Selected individual lines showing similar fluorescence (data normalised against mean of all YFP–TOG12 lines; *n*>6 plants; means ± s.e.m.; blue bars) were analysed in 14-day-old plants by quantitative real-time PCR for *YFP* and endogenous *MOR1* transcript levels (yellow and white bars, respectively). Data were normalised against *YFP-TOG12*; means ± s.e.m., *n*>4 replicates. *Values significantly different from mean *YFP-TOG12* values ($P<0.05$, Student's *t*-test). (**B**) Confocal optical sections, collected with identical collection and processing settings, through root tips of the selected lines demonstrated construct-specific variations in fluorescence. Scale bar: 100 μm. (**C**) Root tips from 7-day-old seedlings of the selected lines were immunolabelled and maximum projections of confocal images of elongating epidermal cells showed transverse microtubules. Scale bar: 20 μm.

transcribed at the same levels as its wild-type counterpart but that the protein was unstable. The endogenous *MOR1* RNA was at wild-type levels (Fig. 2A, white bars) in all transgenic lines. The development of *YFP-TOG12* and *YFP-TOG12^mor1-1* plants was similar to that of wild-type plants and they had comparable growth rates, flowering times and seed set. Microtubule organisation in root epidermal cells was unaffected by the expression of any of the reporter constructs (Fig. 2C).

Transient overexpression of YFP-TOG12^mor1-1 depolymerizes microtubules

To investigate why the YFP–TOG12 constructs did not label microtubules or affect microtubule organisation when stably expressed in *Arabidopsis*, we used biolistic transformation to transiently overexpress them in leek epidermal cells. Within 12 h of particle bombardment, fluorescent cells were observed (Fig. 3). Free YFP localised to the cytoplasm and nucleus (Fig. 3A) whereas
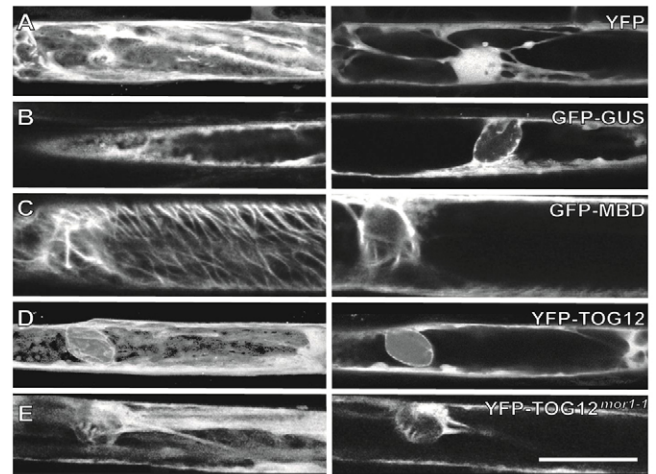

Fig. 3. Transient expression in *Allium* epidermis of YFP–TOG12 fusion proteins. Live-cell confocal imaging shows intracellular localisation of fluorescent reporter proteins. Each panel shows maximum projections of a section adjacent to the plasma membrane (left column) and a median section through the nucleus (right column) from the same cell: (**A**) cytoplasmic YFP, (**B**) GFP–GUS, (**C**) GFP–MBD, (**D**) YFP–TOG12, (**E**) YFP–TOG12^mor1-1. Scale bar: 50 μm.

GUS–GFP, a 96 kDa fusion protein similar in size to YFP–TOG12, remained in the cytoplasm with little nuclear fluorescence (Fig. 3B). Three different microtubule-targeted positive control constructs, GFP–MBD (Fig. 3C), RFP–MBD and GFP–α-tubulin 6 (data not shown), decorated cortical microtubules.

We imaged strongly expressing cells, as well as the weakest expressing cells in which microtubule labelling might be more visible due to a lower cytoplasmic fluorescence. Similar to stable expression in *Arabidopsis*, however, the YFP–TOG12 fragments gave only cytoplasmic fluorescence and did not label microtubules (Fig. 3D). The YFP–TOG12^mor1-1 showed similar cytoplasmic distribution and fluorescence intensity to wild-type YFP–TOG12 (Fig. 3E).

To investigate the effects of TOG12 construct overexpression on microtubules, we immunolabelled transformed leek epidermis with a tubulin-specific antibody and compared the microtubules visible with a Cy-5-tagged secondary antibody in untransformed cells with those in transformed cells in which fixed YFP acted as a marker of transgene expression (Fig. 4). Microtubules in cells transiently expressing cytoplasmic YFP and GUS–GFP were similar to microtubules in surrounding non-transformed cells (Fig. 4A,B). When expressed at high levels, GFP–MBD mildly altered the organisation of microtubule arrays, probably as a consequence of bundle formation (Fig. 4C). Similar results were obtained with RFP–MBD and GFP–TUA6 (data not shown). Microtubule abundance and organisation appeared to be unaffected by the expression of YFP–TOG12 (Fig. 4D). In contrast, the construct containing the *mor1-1* point mutation (YFP–TOG12^mor1-1) caused severe microtubule disruption (Fig. 4E). Compared to adjacent non-transformed cells, cells expressing the YFP–TOG12^mor1-1 construct always had relatively few microtubules that were short and disordered, or lacked microtubules entirely.

Taken together, the live imaging experiments demonstrate that the *mor1-1* point mutation dramatically alters the activity of the reporter protein. The YFP-tagged wild-type TOG12 fragment of
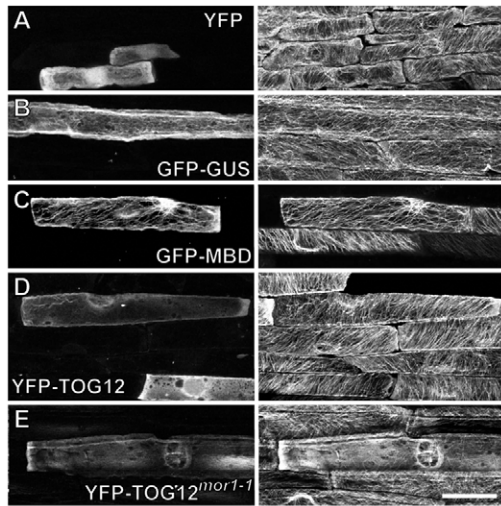
Fig. 4. Immunolabelling of microtubules in leek epidermal cells expressing YFP fusion proteins. Leek leaf epidermal cells expressing YFP fusion proteins were fixed and immunolabelled with monoclonal anti-tubulin antibodies. Maximum projections of confocal optical sections show fixed GFP and YFP fusion proteins (left column) and Cy-5-labelled microtubules (right column) in transformed and surrounding cells. (**A**) YFP, (**B**) GFP–GUS, (**C**) GFP–MBD, (**D**) YFP–TOG12, (**E**) YFP–TOG12^{mor1-1}. Scale bar: 50 μm.

MOR1 could be expressed and sustained at high levels in stably transformed *Arabidopsis* plants or in biolistically transformed leek cells with no consequence to microtubule organisation. In contrast, substituting the leucine residue at position 174 with a phenylalanine resulted in strong post-transcriptional reduction in the reporter protein levels in stably transformed *Arabidopsis* cells and caused disruption of cortical microtubule arrays when transiently overexpressed in the leek epidermal cells.

Based on these results, we hypothesised that N-terminal tagging of TOG12 interferes with its ability to interact with microtubule polymers. We considered two alternative explanations for the disruption of microtubule arrays in the leek epidermal cells expressing the TOG12 with the L174F *mor1-1* point mutation. One hypothesis is that this amino acid substitution increases the affinity of the TOG12 fragment for free tubulin, resulting in sequestration of tubulin subunits in the cytosol and consequent depolymerization of microtubules. Alternatively, the *mor1-1* mutation could enhance microtubule lattice binding, which would prevent multiple polymerase reactions and inhibit the ability of endogenous MOR1 protein to track the growing microtubule ends. In the stably transformed *Arabidopsis* lines, lower protein levels as a result of post-transcriptional degradation apparently protected the microtubules from the same fate. In order to test these hypotheses, we carried out *in vitro* assays of purified TOG12 proteins by expressing and purifying affinity-tagged proteins from bacterial cultures. In addition, we created a C-terminal-tagged TOG12–GFP fusion protein (with and without the *mor1-1* point mutation) to examine whether this construct is able to bind to microtubules and work as a minimal microtubule polymerase.

N-terminal tagging inhibits microtubule polymerization and impedes binding of TOG12 to microtubule polymers
In order to test the hypothesis that N-terminal tagging of TOG12 interferes with its ability to interact with microtubule polymers,

we cloned another version of TOG12 (NTag–TOG12) with a large N-terminal 158 amino acid affinity tag and compared its *in vitro* properties with those of TOG12–His (a small C-terminal six-amino-acid-long histidine tag).

The ability to bind microtubules was determined with a microtubule co-sedimentation assay (supplementary material Fig. S1). Polymerized and taxol-stabilised microtubules at increasing concentrations (0–10 μM) were incubated with TOG12–His and NTag–TOG12 constructs, sedimented by ultracentrifugation and analysed by SDS-PAGE (Fig. 5A, shows 0 and 2.5 μM tubulin). The amount of each protein in the pellet was determined densitometrically and the dissociation constant was calculated by nonlinear regression (Fig. 5B). We calculated a K_d of 1.36 ± 0.32 μM ($\pm$ s.e.m.) for TOG12–His and 2.01 ± 0.30 μM for NTag–TOG12 (Fig. 5B). This shows that N-terminal tagging interferes with binding to taxol-stabilised microtubules.

We next tested the influence of the first two TOG domains on dynamic microtubules. In turbidity assays, tubulin polymerization can be monitored through the ability of microtubules to scatter light, with polymerization kinetics altered by the addition of microtubule/tubulin binding drugs and proteins. The NTag–TOG12 protein showed no significant difference in comparison to the control (Fig. 5C, dashed and solid line, respectively). In contrast, TOG12–His showed a substantial relative increase in polymer mass (Fig. 5C, dotted line). From these results we conclude that N-terminal tagging reduces the affinity of TOG12 for microtubules, which in turn impairs its ability to promote microtubule polymerization.

C-terminal tagging permits TOG12 to bind microtubules and to complement the *mor1-1* phenotype
To confirm our *in vitro* results *in vivo*, we fused the TOG12 to a C-terminal GFP tag and transformed this construct into wild-type and *mor1-1* plants. The expression of this protein was driven by the native MOR1 promoter to avoid overexpression artefacts. Despite many attempts, no TOG12^{mor1-1}–GFP transformants could be recovered. By comparison, the TOG12–GFP wild-type construct yielded 28 independent transgenic lines. This indicates that the TOG12^{mor1-1}–GFP protein is likely to be toxic, resulting in embryo lethality of primary transformants.

Screening 15 independent T2 lines of TOG12–GFP revealed no obvious binding to microtubules and showed a diffuse cytoplasmic localisation of the fusion protein (Fig. 5D; supplementary material Movie 1). In contrast, when TOG12–GFP was transformed into *mor1-1* plants, microtubules were extensively labelled in many cell types including epidermal cells from elongating hypocotyls (Fig. 5D; supplementary material Movie 2). Colocalization with microtubules was confirmed by transiently coexpressing the microtubule reporter mCherry–MAP4-MBD (Gutierrez et al., 2009) in TOG12–GFP/*mor1-1* seedlings (Fig. 5E). This demonstrated that in the *mor1-1* mutant, the TOG12–GFP associated along the entire length of microtubules.

The TOG12–GFP evidently restored normal microtubule dynamics and organisation, suggesting that it can complement the deficiency caused by the *mor1-1* mutation. When grown at 31°C, the microtubule arrays in *mor1-1* pMOR1:TOG12–GFP plants did not undergo disruption (Fig. 5D; supplementary material Movie 3) as expected for *mor1-1* (see Whittington et al., 2001). These results show clearly that the TOG12–GFP is a functional protein and that binding to microtubules is possible with a C-terminal tag.
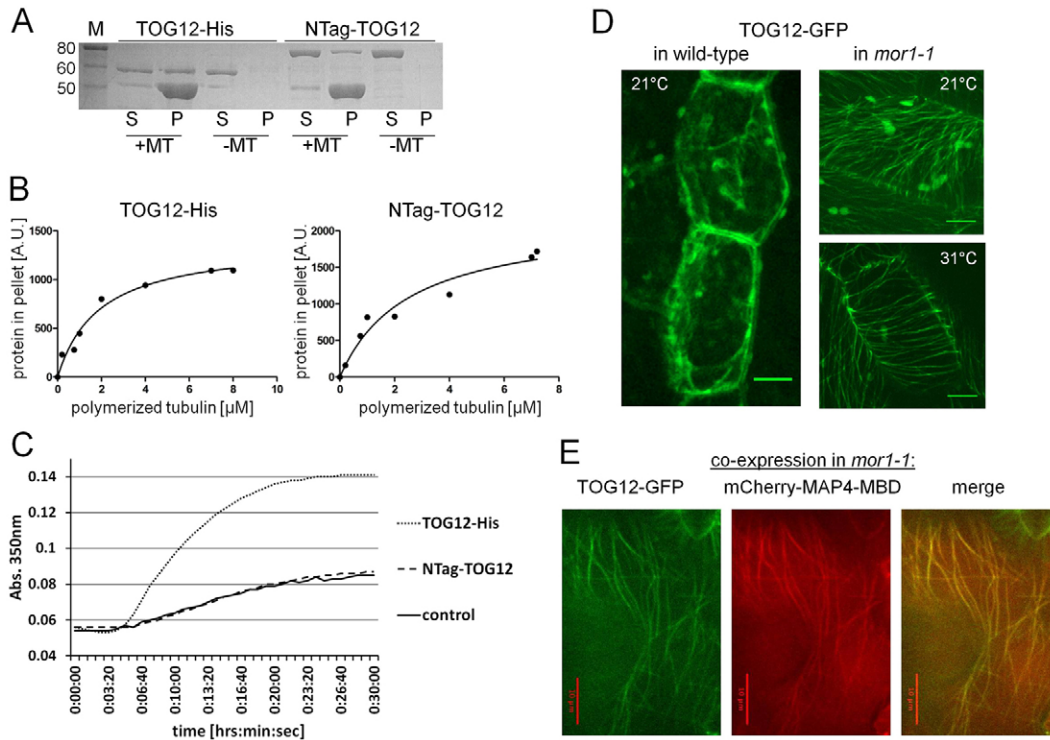
Fig. 5. The influence of N-terminal tags on microtubule binding and polymerization. (**A**) Microtubules were sedimented in the presence of 1 μM TOG12–His or 1 μM NTag–TOG12 (+MT). Controls without microtubules were also sedimented (−MT). Samples of pellet (P) and supernatant (S) (2.5 μM polymerized tubulin) are shown on a SDS-PA gel. The lane labelled M shows molecular mass (kDa) markers. (**B**) The relative amount of each TOG12 protein in the pellet was determined by densitometric measurement and then plotted against the polymerized tubulin concentration. Curve fitting determined the dissociation constant (K_d), as stated in the text. (**C**) The polymerization of tubulin was monitored by measuring the absorbance (turbidity) at 350 nm for 30 minutes. 15 μM tubulin was polymerized in the presence of 2 μM TOG12–His (dotted line) or NTag–TOG12 (dashed line). In the control, no protein other than tubulin was present (solid line). (**D**) TOG12–GFP was stably transformed into wild-type and *mor1-1* plants. Fluorescence microscopy of T2 plants showed mainly cytoplasmic distribution in wild-type plants and microtubule localisation in *mor1-1* plants. The microtubule array was not disrupted by growing the transgenic plants at restrictive temperature for *mor1-1*. (**E**) The localisation of TOG12–GFP to microtubules was confirmed by the transient expression of mCherry–MAP4-MBD in T2 seedlings of TOG12–GFP-transformed plants.

TOG12 binds transiently to tubulin dimers

Using size-exclusion chromatography, we determined that the first two TOG domains can bind transiently to free tubulin. To evaluate a possible interaction, we compared the amount of tubulin in each peak fraction with the amount of tubulin in the same peak fraction of a corresponding run. Because of their elongated structure, TOG domains elute earlier than their molecular weight predicts (van Breugel et al., 2003; Al-Bassam et al., 2006). This elongated shape might be altered upon binding to tubulin and result in a more globular structure. Furthermore, the elution profile of TOG12 constructs was smeared by degradation products (Fig. 6A,B). Therefore, we interpreted the elution profile of tubulin, which is a very pure and globular protein for which binding to another protein will shift the elution to an earlier fraction. We compared the elution profile of tubulin alone (Fig. 6A, black line), TOG12^mor1-1–His (Fig. 6A, blue line) and both proteins mixed (Fig. 6A, red line). The proteins in the peak fractions were separated by SDS-PAGE and the amount of tubulin in each peak fraction was determined by densitometry (Fig. 6C). In the combined run, slightly more tubulin eluted in an earlier fraction than in the run with tubulin alone. This indicates a weak transient binding of TOG12^mor1-1–His to tubulin, but no stable complex formation. The binding of tubulin to the

TOG12–His wild-type construct showed a similar result (supplementary material Fig. S2).

The fact that the wild-type and *mor1-1* TOG12 proteins showed no differences in their affinity for tubulin *in vitro* suggests that the observed depolymerization of microtubules in leek epidermal cells during expression of YFP–TOG12^mor1-1 (Fig. 4E) is not caused by sequestration of tubulin subunits. Interestingly, we found that TOG12^mor1-1 was more vulnerable to degradation and/or aggregation than TOG12, so that the protein had to be loaded quickly after purification. This supports the idea that the low fluorescence of YFP–TOG12^mor1-1 in stably transformed *Arabidopsis* lines (Fig. 2B) is caused by post-translational degradation.

The *mor1-1* point mutation strengthens binding to microtubules

From our size exclusion chromatography analysis, we had to dismiss our hypothesis that the *mor1-1* mutation causes strong binding to tubulin dimers. In order to test our alternative hypothesis that the *mor1-1* point mutation diminishes the ability to promote microtubule growth, we assessed the ability of TOG12^mor1-1–His to bind microtubules and promote their polymerization.
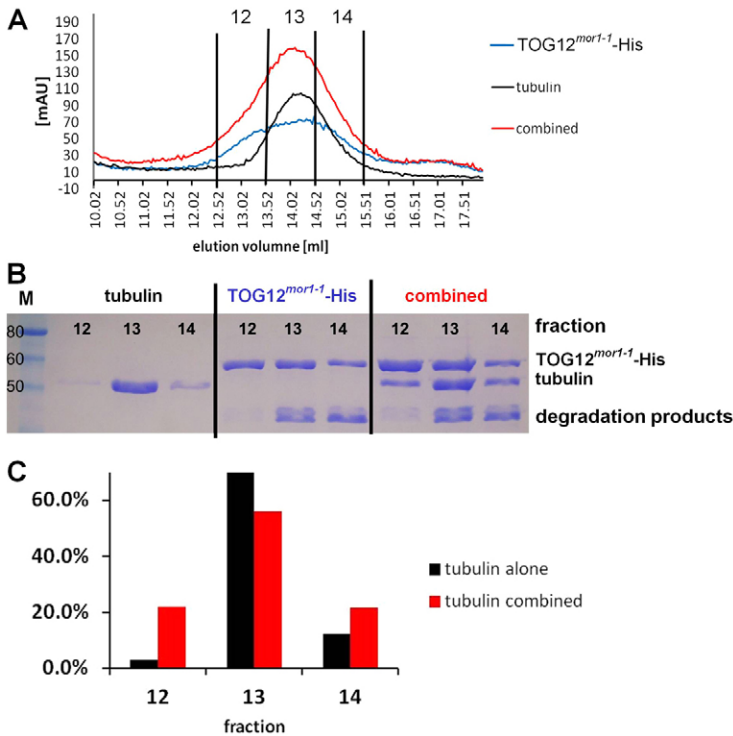
Fig. 6. Size-exclusion chromatography of TOG12^{mor1-1}–His with tubulin. (A) The elution volume on the *x*-axis is plotted against the absorbance at 280 nm on the *y*-axis. 1 ml protein solution of 7.5 µM TOG12^{mor1-1}–His (blue), 3 µM tubulin (black) and both combined (red) were injected onto the column. (B) Peak fractions (12, 13, 14) of all three runs were collected and samples loaded on a SDS-PA gel. M, molecular mass markers (kDa). (C) The percentage of tubulin in each fraction was determined by densitometry. In the experiment with tubulin alone (black), relatively little tubulin was eluted in the early fraction (12) and more in the late fraction (14). When both proteins were combined (red), equal amounts of tubulin were eluted in the early fraction (12) and late fraction (14).

When we co-sedimented TOG12^{mor1-1}–His with taxol-stabilised microtubules, we determined a K_d of 0.48±0.15 µM (±s.e.m.; Fig. 7A,B). This was a drastic increase in microtubule affinity in comparison with the wild-type TOG12–His for which we found a K_d of 1.36±0.32 µM (Fig. 7A,B; Fig. 5A,B). It was interesting to note that, as with the size exclusion experiments, the mor1-1 form of the protein was more vulnerable to degradation but only in control experiments without microtubules.

The influence on dynamic microtubules was tested in turbidity assays. TOG12^{mor1-1}–His did not show significant differences in promoting microtubule polymerization in comparison with the wild-type construct (Fig. 7C). Nevertheless, we cannot exclude the possibility that subtle differences exist, as turbidity assays showed variations between independent protein purifications of the same construct. These might be due to variable amounts of nonfunctional or aggregated proteins in each protein purification, as these cannot be excluded when protein concentration is determined. Technical replicates, however, were highly reproducible. To exclude the possibility that the increase in polymer mass is due to microtubule bundling, we imaged samples with a transmission electron microscope after negative staining. No bundling could be observed in these images (supplementary material Fig. S3).

Taken together, we could confirm our hypothesis that N-terminal tagging lowers the binding affinity of TOG12 to microtubules and its ability to promote microtubule polymerization. We ruled out the possibility that the *mor1-1* point mutation enhanced affinity of TOG12 for free tubulin but instead found that the *mor1-1* point mutation increased the affinity of TOG12 for microtubule polymers. This indicates that the *mor1-1* mutation generates high binding affinity but that this reduces the ability of the first two N-terminal TOG domains to dissociate from microtubules, which would be required to catalyse additional polymerization reactions. By extension, full length MOR1 protein with the L174F mutation

might, at restrictive temperature, lose its ability to diffuse along growing and shrinking microtubules, resulting in less dynamic microtubules.

Discussion

The aim of our study was to better understand the conserved mechanisms by which XMAP215/Dis1 proteins control microtubule dynamics. Consequently, we focussed on analysis of the first two N-terminal TOG domains. Recent studies reinforce the view that these two domains define the function of these essential microtubule polymerase proteins. Widlund et al. (Widlund et al., 2011) found that inactivation of TOG3 and 4 of the *Xenopus* XMAP215 had little effect, while inactivation of TOG1 and 2 almost abolished protein activity. Currie et al. found that TOG12 is able to rescue the Msps depletion phenotype in Drosophila, while TOG34 did not (Currie et al., 2011). Similar to XMAP215 studies (Widlund et al., 2011; Popov et al., 2001), we found that the first two TOG domains of MOR1 are sufficient to promote microtubule assembly *in vitro* and could rescue the *mor1-1* mutant phenotype when expressed *in vivo*. However, in contrast to previous studies in which the first two TOG domains of XMAP215 were found to have high affinity for tubulin but low affinity for microtubules (Popov et al., 2001), our experiments determined that the TOG12 construct of MOR1 binds strongly to microtubules and has a low affinity for tubulin. This striking difference leads us to speculate that there could be substantial differences in the way the first two TOG domains of plant and animal members of the XMAP215/Dis1 family proteins operate and/or that there is an additional microtubule-binding domain at the very N-terminus of MOR1.

Our speculation that there is a novel microtubule-binding domain at the N-terminus of MOR1 is important because, to date, a microtubule-binding domain has not been identified in MOR1 in *Arabidopsis* and other plant homologues. Although Twell et al.
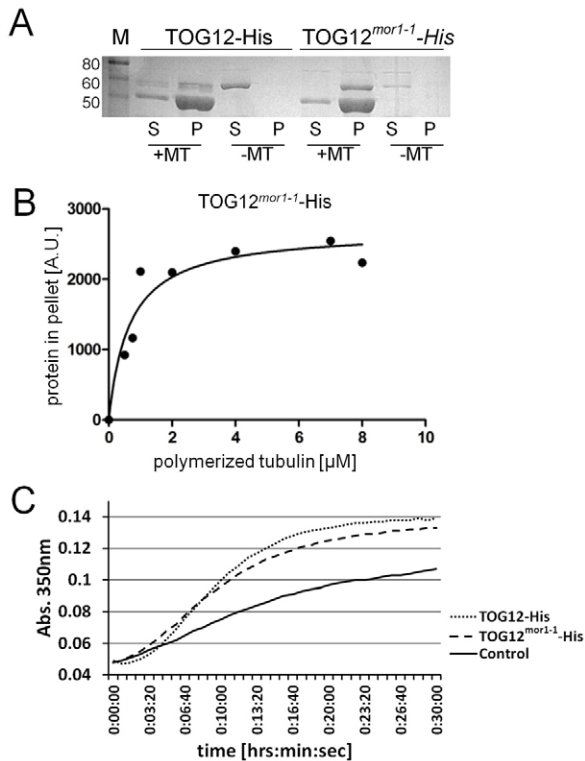
Fig. 7. Influence of the *mor1-1* point mutation on microtubule binding and polymerization. (**A**) Microtubules (2.5 µM) were sedimented in the presence of 1 µM TOG12–His or 1 µM TOG12^{mor1-1}–His (+MT). Controls without microtubules were sedimented as well (−MT). Samples of pellet (P) and supernatant (S) were loaded on an SDS-PA gel. (**B**) Densitometric measurement determined the relative amount of each TOG12 protein in the pellet, which was plotted against the polymerized tubulin concentration. Curve fitting determined the dissociation constant (K_d) as stated in the text. (**C**) The polymerization of tubulin was monitored by measuring absorbance (turbidity) at 350 nm for 30 minutes. 15 µM tubulin was polymerized in the presence of 2 µM TOG12–His (dotted line) or TOG12^{mor1-1}–His (dashed line). In the control, no protein other than tubulin was present (solid line).

reported that a C-terminal fragment of MOR1 was able to bind microtubules *in vitro*, the binding domain was not mapped to a specific motif nor was the relative affinity determined (Twell et al., 2002). A microtubule-binding domain between TOG4 and 5 was found in XMAP215 (Widlund et al., 2011), with the binding capacity of this domain confirmed and another microtubule-binding domain between TOG2 and 3 recently identified in Msps (Currie et al., 2011). As a consensus, Currie et al. proposed that a highly conserved microtubule-binding motif with amino acid sequence exactly matching or similar to 'KLVK' (Currie et al., 2011). We note that a similar sequence is present at the N-terminus of MOR1 ('KLLK'), but not XMAP215, Msps or TOGp (Fig. 8A). This short insert might be important for microtubule binding and could also explain why N-terminal tagging prevents TOG12 from working as a minimal polymerase (Fig. 8B,C). In a future study, we will investigate this by mutating or truncating the putative N-terminal microtubule-binding domain.

Why obvious TOG12–GFP binding to microtubules in the wild-type background is lacking also remains to be solved. This could be due to competition with the endogenous MOR1 protein

and/or the transient nature of binding. Why the endogenous MOR1 with the L174F mutation permits a greater amount of interaction between TOG12–GFP and microtubules remains unclear and will be the focus of future experiments that will address the issue of competition versus cooperation of truncated and full-length mutant and wild-type MOR1 at permissive or restrictive temperature. These experiments will allow us to extend our model to the *in vivo* situation.

The crucial function of the TOG1 domain in microtubule dynamics is underscored by the fact that the MOR1 protein was discovered through a genetic screen that identified temperature-sensitive microtubule disruption as a consequence of three different point mutations in the N-terminal TOG1 domain (Whittington et al., 2001; Konishi and Sugiyama, 2003). Understanding how these single amino acid substitutions cause microtubule disruption is also important for understanding how MOR1 works. In the current study, our *in vitro* assays did not support the possibility that the *mor1-1* point mutation enhances affinity for free tubulin to generate the observed microtubule disruption when YFP–TOG12^{mor1-1} was overexpressed in leek epidermal cells. According to our size exclusion chromatography experiments, the first two TOG domains, with or without the *mor1-1* (L174F) point mutation, only showed weak binding to tubulin dimers, and turbidity assays indicated that TOG12^{mor1-1}–His did not inhibit microtubule polymerization. Instead, our co-sedimentation experiments revealed that the *mor1-1* point mutation increased the affinity of the TOG12 proteins for microtubule polymers. This finding suggests that the *mor1-1* L174F mutation causes mutant protein to bind too strongly to microtubules, and through its inability to track along the microtubule lattice, impedes microtubule growth and shrinkage (illustrated schematically in Fig. 8C). Loss of parallel microtubule order in the *mor1-1* mutant (Whittington et al., 2001) has recently be shown through live imaging and mathematic modelling to result from less frequent microtubule-microtubule encounters, which is one consequence of the sluggish dynamics that cause microtubules to remain relatively short (Kawamura and Wasteneys, 2008; Allard et al., 2010). In the leek epidermal cell overexpression system, the high levels of YFP–TOG12^{mor1-1} might compensate for the hindrance of the N-terminal tag, bind strongly to microtubules and, through interference with microtubule polymerization, generate the observed microtubule disruption.

Why microtubules were not disrupted when YFP–TOG12^{mor1-1} was expressed in the stably transformed *Arabidopsis* plants can be explained by the fact that the fusion proteins were in low abundance. One of the most intriguing observations of our study was that despite being driven by the same constitutive promoter and having almost identical transcript levels to the wild-type *YFP-TOG12* construct, the YFP–TOG12^{mor1-1} protein was almost undetectable. The idea that the YFP–TOG12^{mor1-1} is unstable and readily degraded *in vivo* is supported by our observations that the *mor1-1* point mutation made the TOG12 recombinant protein vulnerable to degradation during preparation of expression protein specifically when not bound to microtubules. Interference with microtubule binding by the N-terminal YFP tag, along with the absence of the C-terminal microtubule-binding sites, presumably exposed the YFP–TOG12^{mor1-1} to proteolytic degradation. In the original *mor1-1* homozygous mutant, full-length protein with the L174F amino acid substitution was detected by immunofluorescence along the
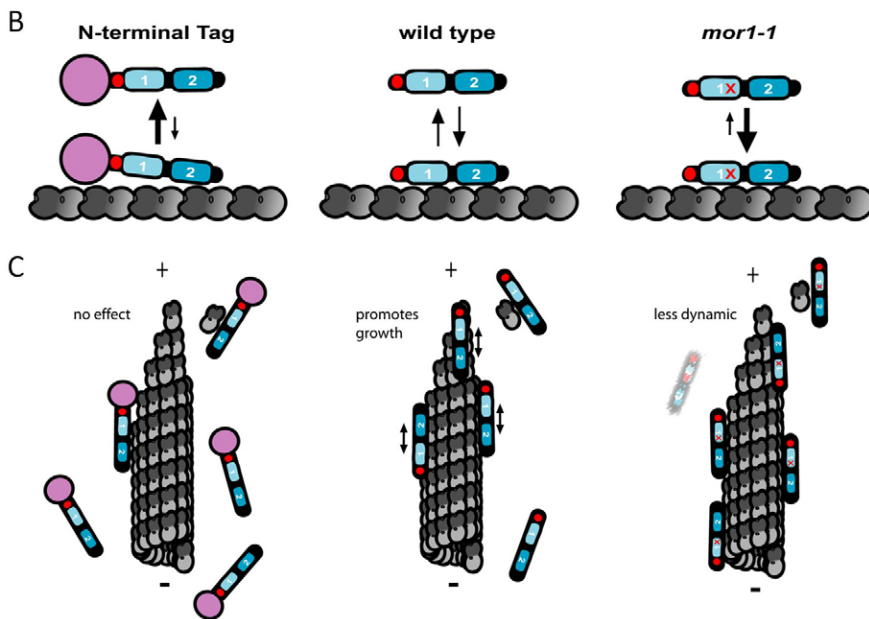
Fig. 8. Putative microtubule-binding domain and interaction with microtubules. (**A**) The N-terminal sequence of MOR1 was aligned with three other representatives of the subgroup with five TOG domains of the XMAP215 family using ClustalW2. MOR1 has an additional insert of five amino acids containing a putative microtubule-binding motif 'KLLK' (red box). (**B**) The model shows the interaction of the first two TOG domains (blue) with a protofilament (grey). The putative microtubule-binding domain is shown in red. The N-terminal tag (purple) inhibits binding to the protofilament, whereas the wild-type construct has moderate affinity. The *mor1-1* point mutation (red X) increases the affinity for microtubules. (**C**) The binding affinity of the TOG12 constructs has different effects on microtubule dynamics *in vitro*. At the microtubule plus-end, constructs with an N-terminal tag have no effect. The wild-type construct can promote microtubule growth and diffuse along the microtubule lattice. Constructs with the *mor1-1* point mutation bind too strongly to microtubules and therefore do not diffuse along the microtubule lattice. TOG12*mor1-1* is unstable when not bound to microtubules (faint version) but when strongly bound to microtubules it inhibits shrinkage.

microtubule lattice even at restrictive temperature (Kawamura and Wasteneys, 2008). This is consistent with the concept that the mutant protein, if bound to microtubules, is less easily degraded and can cause microtubule disruption at the restrictive temperature (Fig. 8C).

Our results not only confirm and complement results from previous studies and let us draw conclusions for a possible microtubule-binding domain in MOR1, they also query if the proposed mechanisms by which members of the XMAP215/Dis1 family work are satisfactory (reviewed by Al-Bassam and Chang, 2011). TOG domains have so far been considered to be responsible for tubulin binding. Microtubule-binding domains are thought to be basic stretches between the TOG domains. How is it then possible that a single point mutation in a TOG domain increases microtubule affinity? As point mutations in the fifth HEAT repeat have not only been found to be deleterious in plant but also in yeast (Wang and Huffaker, 1997), *Drosophila* (Brittle and Ohkura, 2005) and nematode (Bellanger et al., 2007) orthologues, it cannot be considered to be a plant-specific phenomenon. It remains to be investigated which role TOG domains play in microtubule binding and release cycles and whether the fifth HEAT repeat has the power to balance the microtubule affinity of MOR1. Nevertheless, we can conclude from our results that a balanced microtubule affinity in the N-terminal TOG domain is crucial for the polymerase activity of MOR1.

Materials and Methods
Fusion protein constructs
For *in vivo* experiments, *YFP-TOG12* and *YFP-TOG12mor1-1* (aa 1–509) were amplified from cDNA and, at the N-terminus, ligated to YFP sequences and cloned into the plant primary vector pART7 (Gleave, 1992) so that proteins were expressed under the control of the constitutive 35S promoter (Odell et al., 1985). The pART7+YFP vector was used to express unbound, cytosolic YFP as a control. The TOG domains in the TOG12-GFP construct were PCR amplified from cDNA and recombined into a pMDC107 vector (Curtis and Grossniklaus, 2003). The expression *in planta* was driven by the native MOR1 promoter.

For *in vitro* experiments, the same two TOG domains (aa 1–528) were amplified from cDNA and cloned into pET21b vector (Novagen, Merck KGaA, Darmstadt, Germany) for bacterial expression. A C-terminal 6xHis fusion tag was used for affinity purification. An equivalent PCR product (aa 1–526) was cloned into pET32b vector (Novagen, Novagen, Merck KGaA, Darmstadt, Germany), which contained a 18 kDa N-terminal affinity tag including a 6xHis-Tag. The *mor1-1* point mutation was introduced by site-directed mutagenesis (QuikChange II XL Site-Directed Mutagenesis Kit, Agilent Technologies, Santa Clara, CA, USA).

Stable expression
Fusion cassettes were excised from pART7 with *Not*I and sub-cloned into the plant binary vector pART27 (Gleave, 1992). *Arabidopsis* plants were transformed using the floral dip method (Clough and Bent, 1998). Approximately 1000 surface sterilized T1 seeds were screened on 0.7% (w/v) agar plates containing Hoagland's salts, 3% (w/v) sucrose and 50 µg/ml kanamycin. Seeds were grown at 21℃ under constant light (80–100 µE/m²s) for 7–10 days before kanamycin-resistant seedlings were selected on the basis of green cotyledons, true leaf formation and root elongation.

Sterilized T2 seeds from transgenic Col-0 and *mor1-1* plants carrying the MOR1pro::TOG12-GFP construct were sown on Hoagland's medium (3% sucrose and 1.2% bacto-agar) supplemented with 50 µg/ml hygromycin B and stored in the dark for 2 days at 4℃. Seeds were then grown vertically for 5 days in a 21℃ growth cabinet (24 h light). Transgenic plants that were to be observed at the *mor1-1* restrictive temperature were then transferred to a 31℃ growth cabinet (24 h light) for 48 hours.

Quantitative PCR
Total RNA was isolated from pooled seedlings with the Plant RNeasy mini kit (Qiagen, Valencia, CA, USA) and reverse transcribed with SuperScript III Reverse Transcriptase using random rather than oligo dT primers to avoid bias towards shorter transcripts (Invitrogen, Grand Island, NY, USA). The relative amount of specific cDNA templates for *YFP* and *MOR1* were quantified in the different samples with real-time PCR. Primers for *MOR1* (5′-GTAACATGAATCCT-GGAGTGATGAC-3′ and 5′-GCTTGGGGTCTCTAGTTCTACAT-3′) amplified

a 290 bp fragment. These primers replicated from the endogenous gene product, and not from either the transgenes or from genomic DNA contamination. Primers for *YFP* (5′-GAACGGCATCAAGGTGAACT-3′ and 5′-ACGAACTCCAGCA-GGACCAT-3′) amplified a 250 bp fragment. Primers for UBQ10, were used to normalise cDNA levels. The reaction used HotstarTaq PCR kit (Qiagen), monitored by SYBR Green I (Thermo Fisher Scientific, Springfield, NJ, USA) fluorescence. Thermocycling used a Rotorgene 2000 Thermal Cycler (Corbett Research, Sydney, NSW, Australia) with an initial activation step (15 min, 95℃) followed by 35 cycles (denaturation, 30 s, 95℃; annealing, 30 s, 54℃; extension, 30 s, 72℃; fluorescence acquisition, 13 s, 84℃). Specificity of amplification was confirmed through a melt curve analysis of final PCR products, and RNA samples without reverse transcriptase were included to control for genomic DNA contamination. Comparative quantification values were normalised to the YFP–TOG12 sample as the expression of this transgene was of intermediate intensity.

Transient expression in leek

For N-terminal fusion proteins, constructs were expressed transiently in the epidermal cells of 2 cm^2 pieces of leek (*Allium porrum* L.) leaf by particle bombardment (model PDS-1000, 1100 psi rupture discs; Bio-Rad, Regents Park, NSW, Australia) (Collings et al., 2003). Plant tissue was incubated overnight before being imaged or processed for immunofluorescence microscopy (Collings et al., 2002). Controls for the YFP-MOR1 constructs included cytoplasmic YFP, GFP-MBP [based on Marc et al. (Marc et al., 1998)], RFP-MBD and GFP-GUS (pCAMBIA1304).

Transient expression in *Arabidopsis*

To observe colocalisation of TOG12-GFP with microtubules in *Arabidopsis* seedlings, transient expression was performed according to Li et al. (Li et al., 2009). A microtubule reporter construct 35Spro::mCherry:MAP4-MBD (Gutierrez et al., 2009), was transformed using *Agrobacterium tumefaciens* into 5-day-old T2 *mor1-1* seedlings carrying the MOR1pro::TOG12-GFP construct.

Live-cell imaging and quantification

Images of transformed cells were collected with a confocal microscope (SP2; Leica, Wetzlar, Germany) with fourfold line averaging used to reduce noise and stacks of optical sections collected at 1.0 μm intervals. To quantify fluorescence levels in *Arabidopsis* roots, 5-day-old seedlings were imaged on a Zeiss Axiophot microscope (Zeiss, Göttingen, Germany). Average fluorescence was quantified in Metamorph (version 4.1.7, Universal Imaging, Downington, PA, USA) in the region behind the root cap. Low magnification dark field and fluorescence images of *Arabidopsis* plants were taken on a dissecting microscope (MZ FLIII; Leica, Wetzlar, Germany).

Seedlings transformed with TOG12–GFP were imaged using a Perkin Elmer Ultraview VoX Spinning Disc Confocal system (Improvision, Coventry, UK) and a Hamamatsu 9100-02 electron multiplier CCD camera (Hamamatsu, Japan) mounted on a Leica DMI6000 inverted microscope (Leica, Germany). An argon 488 nm laser line with a complementary GFP (525/36) emission band filter or a 561 nm laser with a complementary RFP (595/50) emission band filter was used. Images were taken with either a 40× (oil) or 63× (water) objective. Temperatures of the samples (either at 21℃ or 31℃) were maintained using an objective heater (Bioptechs) and a temperature-controlled stage (Bionomic controller BC-110 equipped with Heat exchanger HEC-400, 20/20 Technology, Inc.). Z-stacks (0.3 μm slices) were acquired of the outer epidermal layers of the hypocotyl or cotyledon. Images were processed using ImageJ (http://rsbweb.nih.gov/ij/).

Immunofluorescence microscopy

Microtubules in *Arabidopsis* roots were immunolabelled with monoclonal anti-tubulin (Sigma clone B512; diluted 1/1000 in incubation buffer; 1 h) and Cy-5-conjugated sheep anti-mouse IgG (Jackson, West Grove, PA, USA; diluted 1/200; 1 h) as previously described (Collings and Wasteneys, 2005).

Electron microscopy

Microtubules were polymerized as described for the turbidity assay (see below), but GTP was supplemented by GMP–CPP (Jena Biosciences, Jena, Germany) for stabilisation. 5 μl of a 1:10 dilution was dried on glow-discharged, formvar-coated copper grids (mesh size 300; Ted Pella, Redding, CA, USA) and stained with 2% uranyl acetate (10 s, Ted Pella). Images were collected with a transmission electron microscope (H-7600 Hitachi High Technologies, Tokyo, Japan).

Recombinant protein purification

Recombinant proteins were expressed in bacterial BL21-CodonPlus-RIL cells (Agilent, Santa Clara, CA, USA) and purified with a Ni-NTA (Qiagen) column in 50 mM sodium phosphate, 250 mM NaCl, 2 mM MgCl$_2$, 250 mM imidazole, pH 7.2. For buffer exchange and desalting, the protein solution was loaded onto a PD midi-trap G25 column (GE Healthcare, Pittsburgh, PA, USA) and eluted with BRB80+ (80 mM PIPES, 5 mM MgCl$_2$, 0.5 mM EGTA, pH 6.9 with KOH). To minimize the residual concentration of imidazole, this step was repeated twice.

Protein purity was assessed by SDS-PAGE and Coomassie staining (SimplyBlue, Safe Stain, Invitrogen). Protein concentration was determined with a Bradford assay (Protein Assay, Bio-Rad, Hercules, CA, USA). All *in vitro* assays were performed with at least with two independent biological replicates and three technical replicates.

Tubulin purification

Tubulin was purified from fresh sheep brains by temperature-dependent polymerization–depolymerization cycles as described first in Borisy et al. (Borisy et al., 1975). A total of four fresh sheep brains were transported on ice from the slaughterhouse to the lab, where meninges and blood vessels were removed. The brains were immediately homogenised in a blender with 500 ml of 100 mM PIPES, 2 mM EGTA, 1 mM MgSO$_4$, 0.1 mM ATP and 1 mM DTT, pH 6.9, and centrifuged at 10,000 rpm in a GSA rotor, Sorvall centrifuge for 60 min at 4℃. The supernatant was decanted into an Erlenmeyer flask and 25% glycerol and 2 mM ATP added. Microtubules were polymerized in a 35℃ water bath for 30 min. Afterwards microtubules were sedimented in a Beckman ultracentrifuge using a 70Ti rotor, at 35,000 rpm for 50 min. The pellet was resuspended in ice-cold PIPES buffer (100 mM PIPES, 1 mM EGTA, 1 mM MgSO$_4$, 1 mM GTP, 1 mM DTT, pH 6.9) and microtubules depolymerised in a glass homogeniser for 25 min. This cycle of polymerization and depolymerisation was repeated two more times. One cycle was in high salt buffer (500 mM PIPES, 2 mM EGTA, 1 mM MgSO$_4$, 1 mM ATP, 1 mM DTT, pH 6.9) to remove microtubule associated proteins. After the last depolymerization step, the tubulin solution was cleared by ultracentrifugation, aliquoted, flash-frozen in liquid nitrogen and stored at −80℃. All animal experiments were performed according to approved guidelines.

Gel filtration chromatography

For gel filtration experiments, an AKTA purifier FPLC (GE Healthcare) maintained at 4℃ was used and a Superdex 200 10/300 GL column (GE) was equilibrated in running buffer. To exclude the influence of salt and buffer conditions, replicates were repeated in three different buffers: (1) 20 mM PIPES, 200 mM KCl, 2 mM MgCl$_2$, 1 mM EGTA, 1 mM DTT, 50 μM GTP, pH 6.9; (2) 25 mM Tris HCl, 75 mM NaCl, 1 mM MgCl$_2$, 1 mM EGTA, 1 mM DTT, pH 7.3; (3) 80 mM PIPES, 150 mM KCl, 5 mM MgCl$_2$, 1 mM EGTA, 1 mM DTT, 50 μM GTP, pH 6.0. The column was calibrated with standard protein of known molecular mass (MWGF200, Sigma-Aldrich). A 1 ml probe containing 1 μM tubulin dimers and/or 1–3 μM TOG12 was injected after 10 min incubation on ice. The concentration of recombinant protein varied slightly, because it was injected as soon as possible after purification to minimize degradation. The concentration was determined subsequently. With a flow rate of 0.2 ml/min, we collected 1.5 ml fractions and analysed them by SDS-PAGE. The percentage of each protein in each fraction was determined by densitometric measurement, setting on 'uncalibrated OD' (Gel analyzer, ImageJ).

Microtubule co-sedimentation assay

Tubulin was polymerized by the addition of 1 mM GTP and incubation at 37℃ for 20 min. Microtubules were stabilised by the addition of 20 μM taxol and subsequent incubation at 37℃ for 20 min. Recombinant proteins (1 μM final concentration) were incubated with increasing amounts of (0–10 μM polymerized tubulin) microtubules in BRB80+ buffer at room temperature. The reaction mix (100 μl) was sedimented in an Optima TLX ultracentrifuge (TLA100.3 Rotor, Beckman Coulter, Brea, CA, USA) for 15 min at 32℃ and 70,000 rpm. The supernatant was collected immediately after the centrifuge stopped and the pellet resuspended in 100 μl resuspension buffer. Samples of the supernatant and pellet were analysed with SDS-PAGE. The relative amount of each protein in the pellet was determined by densitometric measurement, setting on 'uncalibrated OD' (ImageJ, Gel Analyzer). We only analysed the pellet because the TOG12^{mor1-1}–His protein was unstable when not bound to microtubules and we wanted to be able to compare the values of all proteins investigated. The dissociation constant (K_d) was determined by curve fitting (GraphPad Prism 5.0) and the mean of three independent experiments calculated.

Turbidity assay

Purified proteins (2 μM) were mixed on ice with 15 μM tubulin, 25% glycerol, 1 mM GTP in BRB80+ and 80 μl of each reaction was transferred to a half-area UV-96-well plate (Greiner Bio-One, Monroe, NC, USA). Microtubule polymerization was started simultaneously by a temperature shift to 35℃ and monitored at 350 nm in 50 sec intervals for 30 min in a plate reader (Synergy HT, BioTek, Winooski, VT, USA).

Journal of Cell Science

technical support, and Mathias Schuetz (UBC) for helping with tubulin purification. We thank Joerg Bohlmann, Beverley Green and Brian Ellis (UBC) for access to instruments; Elke Rosche (Australian National University; ANU) for assistance with quantitative PCR and Spencer Whitney (ANU) for the use of a gene gun. We also thank Angela Ho and Jan Marc (University of Sydney) for the GFP- and RFP-MBP constructs, Takashi Hashimoto (Nara Institute of Science and Technology) for GFP-TUA6, Jelmer Lindeboom (University of Wageningen) for 35S:mCherry-MAP4 MBD, and CAMBIA (Canberra) for pCAMBIA1304, and Meadows Valley Meats Ltd. for providing sheep brains for tubulin preparations. The Kazusa DNA Research Institute (Chiba, Japan) provided cDNA clones. The Arabidopsis Biological Resource Center (Columbus, OH, USA) provided a cDNA library.

Supplementary material available online at
http://jcs.biologists.org/lookup/suppl/doi:10.1242/jcs.107045/-/DC1

References

Al-Bassam, J. and Chang, F. (2011). Regulation of microtubule dynamics by TOG-domain proteins XMAP215/Dis1 and CLASP. *Trends Cell Biol.* **21**, 604-614.

Al-Bassam, J., van Breugel, M., Harrison, S. C. and Hyman, A. (2006). Stu2p binds tubulin and undergoes an open-to-closed conformational change. *J. Cell Biol.* **172**, 1009-1022.

Al-Bassam, J., Larsen, N. A., Hyman, A. A. and Harrison, S. C. (2007). Crystal structure of a TOG domain: conserved features of XMAP215/Dis1-family TOG domains and implications for tubulin binding. *Structure* **15**, 355-362.

Allard, J. F., Wasteneys, G. O. and Cytrynbaum, E. N. (2010). Mechanisms of self-organization of cortical microtubules in plants revealed by computational simulations. *Mol. Biol. Cell* **21**, 278-286.

Bellanger, J. M., Carter, J. C., Phillips, J. B., Canard, C., Bowerman, B. and Gönczy, P. (2007). ZYG-9, TAC-1 and ZYG-8 together ensure correct microtubule function throughout the cell cycle of C. elegans embryos. *J. Cell Sci.* **120**, 2963-2973.

Borisy, G. G., Marcum, J. M., Olmsted, J. B., Murphy, D. B. and Johnson, K. A. (1975). Purification of tubulin and associated high molecular weight proteins from porcine brain and characterization of microtubule assembly in vitro. *Ann. N. Y. Acad. Sci.* **253**, 107-132.

Brittle, A. L. and Ohkura, H. (2005). Mini spindles, the XMAP215 homologue, suppresses pausing of interphase microtubules in Drosophila. *EMBO J.* **24**, 1387-1396.

Brouhard, G. J., Stear, J. H., Noetzel, T. L., Al-Bassam, J., Kinoshita, K., Harrison, S. C., Howard, J. and Hyman, A. A. (2008). XMAP215 is a processive microtubule polymerase. *Cell* **132**, 79-88.

Charrasse, S., Schroeder, M., Gauthier-Rouviere, C., Ango, F., Cassimeris, L., Gard, D. L. and Larroque, C. (1998). The TOGp protein is a new human microtubule-associated protein homologous to the Xenopus XMAP215. *J. Cell Sci.* **111**, 1371-1383.

Clough, S. J. and Bent, A. F. (1998). Floral dip: a simplified method for Agrobacterium-mediated transformation of Arabidopsis thaliana. *Plant J.* **16**, 735-743.

Collings, D. A. and Wasteneys, G. O. (2005). Actin microfilament and microtubule distribution patterns in the expanding root of Arabidopsis thaliana. *Can. J. Bot.* **83**, 579-590.

Collings, D. A., Harper, J. D. I., Marc, J., Overall, R. L. and Mullen, R. T. (2002). Life in the fast lane: actin-based motility of plant peroxisomes. *Can. J. Bot.* **80**, 430-441.

Collings, D. A., Harper, J. D. I. and Vaughn, K. C. (2003). The association of peroxisomes with the developing cell plate in dividing onion root cells depends on actin microfilaments and myosin. *Planta* **218**, 204-216.

Currie, J. D., Stewman, S., Schimizzi, G., Slep, K. C., Ma, A. and Rogers, S. L. (2011). The microtubule lattice and plus-end association of Drosophila Mini spindles is spatially regulated to fine-tune microtubule dynamics. *Mol. Biol. Cell* **22**, 4343-4361.

Curtis, M. D. and Grossniklaus, U. (2003). A gateway cloning vector set for high-throughput functional analysis of genes in planta. *Plant Physiol.* **133**, 462-469.

Eleftheriou, E. P., Baskin, T. I. and Hepler, P. K. (2005). Aberrant cell plate formation in the Arabidopsis thaliana microtubule organization 1 mutant. *Plant Cell Physiol.* **46**, 671-675.

Gard, D. L., Becker, B. E. and Josh Romney, S. (2004). MAPping the eukaryotic tree of life: structure, function, and evolution of the MAP215/Dis1 family of microtubule-associated proteins. *Int. Rev. Cytol.* **239**, 179-272.

Gleave, A. P. (1992). A versatile binary vector system with a T-DNA organisational structure conducive to efficient integration of cloned DNA into the plant genome. *Plant Mol. Biol.* **20**, 1203-1207.

Gutierrez, R., Lindeboom, J. J., Paredez, A. R., Emons, A. M. and Ehrhardt, D. W. (2009). Arabidopsis cortical microtubules position cellulose synthase delivery to the plasma membrane and interact with cellulose synthase trafficking compartments. *Nat. Cell Biol.* **11**, 797-806.

Hamada, T., Igarashi, H., Itoh, T. J., Shimmen, T. and Sonobe, S. (2004). Characterization of a 200 kDa microtubule-associated protein of tobacco BY-2 cells, a member of the XMAP215/MOR1 family. *Plant Cell Physiol.* **45**, 1233-1242.

Hamada, T., Itoh, T. J., Hashimoto, T., Shimmen, T. and Sonobe, S. (2009). GTP is required for the microtubule catastrophe-inducing activity of MAP200, a tobacco homolog of XMAP215. *Plant Physiol.* **151**, 1823-1830.

Kawamura, E. and Wasteneys, G. O. (2008). MOR1, the Arabidopsis thaliana homologue of Xenopus MAP215, promotes rapid growth and shrinkage, and suppresses the pausing of microtubules in vivo. *J. Cell Sci.* **121**, 4114-4123.

Kawamura, E., Himmelspach, R., Rashbrooke, M. C., Whittington, A. T., Gale, K. R., Collings, D. A. and Wasteneys, G. O. (2006). MICROTUBULE ORGANIZATION 1 regulates structure and function of microtubule arrays during mitosis and cytokinesis in the Arabidopsis root. *Plant Physiol.* **140**, 102-114.

Konishi, M. and Sugiyama, M. (2003). Genetic analysis of adventitious root formation with a novel series of temperature-sensitive mutants of Arabidopsis thaliana. *Development* **130**, 5637-5647.

Li, J. F., Park, E., von Arnim, A. G. and Nebenführ, A. (2009). The FAST technique: a simplified Agrobacterium-based transformation method for transient gene expression analysis in seedlings of Arabidopsis and other plant species. *Plant Methods* **5**, 6.

Marc, J., Granger, C. L., Brincat, J., Fisher, D. D., Kao, T., McCubbin, A. G. and Cyr, R. J. (1998). A GFP-MAP4 reporter gene for visualizing cortical microtubule rearrangements in living epidermal cells. *Plant Cell* **10**, 1927-1940.

Odell, J. T., Nagy, F. and Chua, N. H. (1985). Identification of DNA sequences required for activity of the cauliflower mosaic virus 35S promoter. *Nature* **313**, 810-812.

Popov, A. V., Pozniakovsky, A., Arnal, I., Antony, C., Ashford, A. J., Kinoshita, K., Tournebize, R., Hyman, A. A. and Karsenti, E. (2001). XMAP215 regulates microtubule dynamics through two distinct domains. *EMBO J.* **20**, 397-410.

Slep, K. C. and Vale, R. D. (2007). Structural basis of microtubule plus end tracking by XMAP215, CLIP-170, and EB1. *Mol. Cell* **27**, 976-991.

Tournebize, R., Popov, A., Kinoshita, K., Ashford, A. J., Rybina, S., Pozniakovsky, A., Mayer, T. U., Walczak, C. E., Karsenti, E. and Hyman, A. A. (2000). Control of microtubule dynamics by the antagonistic activities of XMAP215 and XKCM1 in Xenopus egg extracts. *Nat. Cell Biol.* **2**, 13-19.

Twell, D., Park, S. K., Hawkins, T. J., Schubert, D., Schmidt, R., Smertenko, A. and Hussey, P. J. (2002). MOR1/GEM1 has an essential role in the plant-specific cytokinetic phragmoplast. *Nat. Cell Biol.* **4**, 711-714.

van Breugel, M., Drechsel, D. and Hyman, A. (2003). Stu2p, the budding yeast member of the conserved Dis1/XMAP215 family of microtubule-associated proteins is a plus end-binding microtubule destabilizer. *J. Cell Biol.* **161**, 359-369.

Wang, P. J. and Huffaker, T. C. (1997). Stu2p: A microtubule-binding protein that is an essential component of the yeast spindle pole body. *J. Cell Biol.* **139**, 1271-1280.

Wasteneys, G. O. and Ambrose, J. C. (2009). Spatial organization of plant cortical microtubules: close encounters of the 2D kind. *Trends Cell Biol.* **19**, 62-71.

Whittington, A. T., Vugrek, O., Wei, K. J., Hasenbein, N. G., Sugimoto, K., Rashbrooke, M. C. and Wasteneys, G. O. (2001). MOR1 is essential for organizing cortical microtubules in plants. *Nature* **411**, 610-613.

Widlund, P. O., Stear, J. H., Pozniakovsky, A., Zanic, M., Reber, S., Brouhard, G. J., Hyman, A. A. and Howard, J. (2011). XMAP215 polymerase activity is built by combining multiple tubulin-binding TOG domains and a basic lattice-binding region. *Proc. Natl. Acad. Sci. USA* **108**, 2741-2746.